Mon. Not. R. Astron. Soc. **381,** 797–808 (2007) doi:10.1111/j.1365-2966.2007.12281.x

Frequency-dependent time delays for strong outbursts in selected blazars from the Metsähovi and UMRAO monitoring data bases – II

T. B. Pyatunina,[1⋆] N. A. Kudryavtseva,[2,3†] D. C. Gabuzda,[4‡] S. G. Jorstad,[3,5] M. F. Aller,[6] H. D. Aller[6] and H. Teräsranta[7]

[1]*Institute of Applied Astronomy of the RAS, Zhdanovskaya St 8, 197110, St Petersburg, Russia*
[2]*Max-Plank-Institut für Radioastronomie, Auf dem Hügel 69, 53121 Bonn, Germany*
[3]*St Petersburg State University, Universitetskii pr. 28, Petrodvoretz, 198504, St Petersburg, Russia*
[4]*Physics Department, University College Cork, Cork, Ireland*
[5]*Institute for Astrophysical Research, Boston University, Boston, MA 02215, USA*
[6]*Astronomy Department, University of Michigan, Ann Arbor, MI 48109, USA*
[7]*Metsähovi Radio Observatory, Helsinki University of Technology, Finland*

Accepted 2007 July 25. Received 2007 July 23; in original form 2006 May 19

ABSTRACT

We analyse the radio light curves of the blazars 1308+326, 2223−052 and 2251+158 using University of Michigan Radio Observatory and Metsähovi Radio Observatory multifrequency monitoring data combined with high-resolution very long baseline interferometry (VLBI) observations in order to extract the properties of prominent outbursts. The outbursts are classified as 'core' and 'jet' events according to their behaviour at different frequencies and their associations with features appearing in the VLBI jet. We define the activity cycle for each blazar as the time interval between successive 'core' outbursts. The durations of the activity cycle derived in this way are $\geqslant$14 yr for 1308+326, $\sim$12 yr for 2223−052 and 12.4 $\pm$ 0.6 yr for 2251+158. We find an unusual frequency dependence for the time profiles for a major flare in 1308+326, which may provide evidence for acceleration or bending of the jet flow in the optically thick part of the emission region. Analysis of these activity cycles, combined with our earlier results, leads us to suggest that more luminous blazars possess shorter activity cycles, consistent with the accretion rates being higher in more powerful sources (relative to the Eddington rate).

Key words: galaxies: active – galaxies: jets – quasars: individual: 1308+326 – quasars: individual: 2223−052 (3C 446) – quasars: individual: 2251+158 (3C454.3).

1 INTRODUCTION

The high sensitivity and efficiency of the Very Large Baseline Array (VLBA) have produced unique surveys of radio jets of active galactic nuclei (AGN) (e.g. Kellermann et al. 2004) and bright blazars (Gómez et al. 2001; Homan et al. 2001; Jorstad et al. 2001, 2005; Wehrle et al. 2001). With superb time (as short as 1 month) and angular (down to $\sim$0.1 mas) resolutions, these surveys have significantly improved our understanding of the role that jets play in the nuclear activity. The majority of radio outbursts are associated with the emergence of very long baseline interferometry (VLBI) components in the radio jets (e.g. Savolainen et al. 2002), although the observations together with numerical simulations of relativistic jets (e.g. Aloy et al. 2003) show that the widely used 'one shock = one component' model is an oversimplistic idealization of the perturbations propagating in the jets. The hypothesis that there may exist cycles in the variability of AGN has initiated searches for periodicity in both optical and radio light curves, and resulted in reports of quasi-periodic behaviour in some sources (e.g. Kidger 2000; Pursimo et al. 2000; Raiteri et al. 2001).

In our previous paper (Pyatunina et al. 2006, hereafter Paper I), we performed an analysis of total flux and spectral variability based on multifrequency light curves combined with observed structural changes in the VLBI images of four 'blazars' – AGN displaying dramatic and sometimes rapid variability in total intensity and polarization over a wide range of wavelengths. We suggested that the activity of blazars can be characterized by two parameters: the time-scale for activity of the central engine, $T_{\rm act}$, and the time-scale for evolution of the jet, $T_{\rm evol}$, which is associated with the initial

⋆This was the last paper on which Tamara Borisovna Pyatunina worked before her death in 2005 August.
†Member of the International Max-Planck Research School (IMPRS) for Radio and Infrared Astronomy at the Universities of Bonn and Cologne.
‡E-mail: gabuzda@phys.ucc.ie

appearance of a primary perturbation at the base of the jet and its subsequent dissipation into the quiescent jet downstream. We proposed that T_{act} determines an 'activity cycle' for the source, which can be defined as the time interval between two successive 'core' (optically thick) outbursts, which occur increasingly later at lower and lower frequencies. Between these core events, the source exhibits 'jet' (optically thin) outbursts, which occur synchronously at all frequencies, and can often be associated with the emergence and propagation of VLBI components in the jet. However, our results from Paper I show that pure 'core' or 'jet' outbursts are rare: most outbursts demonstrate both low-frequency time lags and a connection with the ejection of superluminal knots. Nevertheless, our approach allowed us to determine activity cycles with durations of ∼4 yr in 0202+149 and 0059+581 (Pyatunina et al. 2000, 2003), ∼8 yr in 2230+114 and ∼14 yr in 0528+134 (Paper I). Other studies have suggested the existence of activity cycles in the blazars 0420−014 (∼14 yr; Zhou et al. 2000) and 0735+178 (∼12 yr; Agudo et al. 2002). Searching for activity cycles is important for testing theoretical models (e.g. the binary black hole model for the central engine; Lehto & Valtonen 1996), studying properties of the central engine (e.g. searching for correlations between the black hole mass and activity-cycle duration) and predicting future prominent outbursts.

Here, we analyse multifrequency light curves of the three additional blazars 1308+326 (OP313), 2223−052 (3C 446) and 2251+158 (3C 454.3). This choice of blazars for our study is based on the existence of long-term light curves at high and low radio frequencies, as well as contemporaneous, relatively regular VLBI observations.

2 DATA ANALYSIS

As in Paper I, we use the combined data from the University of Michigan Radio Astronomy Observatory (UMRAO; 4.8, 8 and 14.5 GHz (Aller et al. 1985) and the Metsähovi Radio Observatory (MRO; 22 and 37 GHz; Teräsranta et al. 1998, 2004, 2005), which provide us with radio light curves from 4.8 to 37 GHz covering time intervals up to ∼25 years. These data are supplemented by mm data (Steppe et al. 1988, 1992, 1993; Reuter et al. 1997). We determined long-term trends in the light curves by performing a linear interpolation between the deepest minima in the flux density, and then visually searched the light curves for outburst events after subtraction of the long-term trends. Identified events were then decomposed into Gaussian components. The Gaussian decomposition was stopped when the fitted peaks became smaller than 0.15 Jy for 4.8 GHz, 0.3 Jy for 8 GHz, 0.4 Jy for 14.5 and 22 GHz and 0.6 Jy for 37 GHz; the different values of these thresholds are due to the different variability amplitudes at these frequencies.

Tables 1–3 list the parameters of the Gaussian components derived in this way. The columns of the tables give the (1) component designation, (2) observing frequency, (3) epoch of maximum flux, (4) maximum amplitude, (5) full width at half-maximum (FWHM) of the Gaussian component corresponding to the outburst Θ, (6) time delay between the epoch of maximum flux for the outbursts at the given frequency and the corresponding epoch at the highest available frequency ΔT and (7) dispersion determined by the data and Gaussian fit σ^2. These tables include all the fitted Gaussians except for those for a small number of outbursts that were detected at fewer than three frequencies (so that it is difficult to judge the reliability of the corresponding time delays); outbursts whose fitted Gaussians are not presented in the tables on this basis include flares in 1978.47 and 1980.21 for 1308+326; 1981.8 and 1980.43 for 2223-052; 1974.51, 1975.82, 1977.20 and 1980.50 for 2251+158. Fig. 1 shows our decomposition of the complex outburst *B*1 in 2223−052 (see Table 2) into three suboutbursts with Gaussian profiles as an example. As we can see from the tables, a few events are not fit well by Gaussian components owing to either insufficient data or non-Gaussian shapes of the outburst profiles. In all, roughly 8.5 per cent of the outburst-profile fits did not yield reduced χ^2 values less than 0.5.

3 1308+326 (OP313)

The blazar 1308+326 ($z = 0.996$) has properties of both optically violently variable (OVV) quasars and BL Lac objects (Gabuzda et al. 1993). It displays the featureless optical spectrum typical of BL Lac objects (Stickel et al. 1991), together with the powerful extended emission from edge-brightened arcsec lobes (Ulvestad, Johnston & Weiler 1983; Kollgaard et al. 1992), rapid superluminal motion (Kellermann et al. 2004; Lister 2005, $\beta_{app} \approx$ 16–23 c) and high VLBI core brightness temperature (Lähteenmäki & Valtaoja 1999) typical of OVV quasars.

The light curves of 1308+326 at frequencies from 4.8 to 90 GHz are shown in Fig. 2. We estimated the long-term trends in these light curves via linear interpolation between the local/global minima of the light curves in 1981, 1987–1988 and 2000. Table 1 lists the parameters for the Gaussian decomposition after subtraction of these trends.

The light curves display two complex outbursts. The first, observed from 1980 to 1988, consists of four fairly narrow features ('flares' *A*, *B*, *C* and *D*). These flares display moderate (⩽0.3 yr) time lags between their maxima at 4.8 and 14.5 GHz (Fig. 3, left-hand panel). Unfortunately, time lags can be determined relative to the 37 GHz maxima only for flares *B* and *D*, owing to the sparsity of the data at the high frequencies. Note, however, that the time lags between 4.8 and 37 GHz for these two events are only slightly longer (⩽0.4 yr) than the time lags between 4.8 and 14.5 GHz (⩽0.4 yr), suggesting that our analysis suffers little from the relative sparsity of the 37 GHz data.

The second outburst (1988–2001) displays three flares, denoted by *E*, *F* and *G*, which are overlaid on the very prolonged suboutburst *H*, which has its maximum near 1996. The time lags for flares *E*, *F* and *G* are <0.5 yr, similar to the time lags for flares *A*, *B*, *C* and *D*, while the time lag for the extended event *H* reaches ∼1 yr between 37 and 4.8 GHz, with the maxima at 14.5 and 37 GHz being nearly simultaneous (Fig. 3, right-hand panel). The difference in the time lags for the suboutburst and flares may reflect the locations of the emission regions where these events originate. We believe that suboutburst *H* is connected with the optically thick base of the jet where the primary perturbation occurs, while flares *E*, *F* and *G* may have been generated near the front edge of a shock associated with the propagation of the primary perturbation down the jet. The suboutburst peaks when the perturbation reaches that part of the jet when the optical depth is roughly unity. The VLBA 15-GHz survey contains images of 1308+326 at five epochs from 1995 April to 2001 December (http://www.cv.nrao.edu/2cmVLBA/data). These images show a gradual decrease of the core flux density from 4 to 1.7 Jy beam^{-1}, as well as the appearance of a bright superluminal feature ejected in 1995.08 ± 0.01 along position angle PA∼ −80° (Kellermann et al. 2004). The time of the ejection coincides within 0.3 yr with the maximum of suboutburst *H* at 14.5 GHz. Suboutburst

Table 1. 1308+326: parameters of outbursts.

Comp.	Freq. (GHz)	Amplitude (Jy)	T_{max} (yr)	Θ (yr)	Time delay (yr)	σ^2
A	14.5	1.40 ± 0.02	1982.41 ± 0.01	0.65 ± 0.01	0.00 ± 0.01	0.04
	8.0	1.00 ± 0.02	1982.44 ± 0.01	0.62 ± 0.01	0.03 ± 0.02	0.02
	4.8	0.47 ± 0.02	1982.51 ± 0.01	0.72 ± 0.01	0.10 ± 0.02	0.02
B	36.8	2.89 ± 0.19	1983.61 ± 0.02	0.66 ± 0.03	0.00 ± 0.02	0.58
	14.5	2.35 ± 0.03	1983.73 ± 0.01	1.06 ± 0.01	0.12 ± 0.02	0.16
	8.0	1.48 ± 0.02	1983.83 ± 0.04	1.40 ± 0.04	0.22 ± 0.05	0.04
	4.8	0.82 ± 0.02	1983.99 ± 0.08	1.87 ± 0.11	0.38 ± 0.08	0.03
C	14.5	3.40 ± 0.03	1985.55 ± 0.01	0.67 ± 0.01	0.00 ± 0.01	0.09
	8.0	2.61 ± 0.03	1985.61 ± 0.01	0.71 ± 0.01	0.06 ± 0.02	0.06
	4.8	1.57 ± 0.02	1985.78 ± 0.01	0.73 ± 0.01	0.23 ± 0.02	0.01
D	36.8	1.98 ± 0.06	1986.45 ± 0.02	0.96 ± 0.01	0.00 ± 0.02	0.03
	14.5	2.16 ± 0.02	1986.57 ± 0.01	0.92 ± 0.01	0.12 ± 0.02	0.03
	8.0	1.70 ± 0.02	1986.69 ± 0.01	1.02 ± 0.01	0.24 ± 0.02	0.03
	4.8	1.13 ± 0.02	1986.87 ± 0.02	1.06 ± 0.01	0.42 ± 0.03	0.02
E	22.2	0.85 ± 0.15	1988.81 ± 0.03	0.55 ± 0.04	0.00 ± 0.03	0.06
	14.5	0.63 ± 0.01	1988.90 ± 0.01	0.74 ± 0.01	0.09 ± 0.03	0.01
	8.0	0.48 ± 0.02	1988.97 ± 0.02	0.73 ± 0.02	0.16 ± 0.04	0.01
	4.8	0.19 ± 0.01	1989.24 ± 0.03	0.50 ± 0.03	0.43 ± 0.04	0.01
F	36.8	1.89 ± 0.02	1990.38 ± 0.02	1.48 ± 0.02	0.00 ± 0.02	0.07
	22.2	1.44 ± 0.05	1990.47 ± 0.04	1.79 ± 0.04	0.09 ± 0.05	0.07
	14.5	1.73 ± 0.01	1990.65 ± 0.01	1.51 ± 0.01	0.27 ± 0.02	0.03
	8.0	1.77 ± 0.02	1990.73 ± 0.01	1.52 ± 0.01	0.35 ± 0.02	0.03
	4.8	0.68 ± 0.01	1990.83 ± 0.01	1.65 ± 0.01	0.45 ± 0.02	0.02
G	36.8	1.29 ± 0.03	1992.07 ± 0.02	1.28 ± 0.02	0.00 ± 0.02	0.07
	22.2	1.45 ± 0.06	1992.26 ± 0.02	0.92 ± 0.02	0.19 ± 0.03	0.09
	14.5	1.49 ± 0.02	1992.29 ± 0.01	1.13 ± 0.01	0.22 ± 0.02	0.05
	8.0	2.21 ± 0.02	1992.37 ± 0.01	1.31 ± 0.01	0.30 ± 0.02	0.03
	4.8	1.40 ± 0.01	1992.56 ± 0.01	1.21 ± 0.01	0.49 ± 0.02	0.04
H	36.8	2.66 ± 0.03	1994.58 ± 0.03	5.47 ± 0.07	0.00 ± 0.03	0.06
	22.2	3.01 ± 0.02	1994.63 ± 0.04	6.60 ± 0.10	0.05 ± 0.05	0.06
	14.5	3.00 ± 0.02	1994.67 ± 0.01	5.79 ± 0.18	0.09 ± 0.03	0.03
	8.0	3.39 ± 0.02	1995.37 ± 0.02	4.64 ± 0.04	0.79 ± 0.04	0.02
	4.8	2.88 ± 0.01	1995.64 ± 0.01	4.85 ± 0.02	1.06 ± 0.03	0.02
I	36.8	0.78 ± 0.06	1998.71 ± 0.14	0.92 ± 0.31	0.00 ± 0.14	0.10
	22.2	0.49 ± 0.02	1998.73 ± 0.03	0.70 ± 0.07	0.02 ± 0.14	0.04
	14.5	0.90 ± 0.02	1998.62 ± 0.02	0.64 ± 0.03	-0.09 ± 0.14	0.04
	8.0	1.15 ± 0.02	1998.76 ± 0.03	0.52 ± 0.02	0.05 ± 0.14	0.04
	4.8	0.95 ± 0.02	1998.97 ± 0.02	0.60 ± 0.019	0.26 ± 0.14	0.02

H has a very broad profile at all frequencies ($\Theta \sim 5$ yr). This profile width nominally implies a size for the excited region of $\Theta\delta \sim 180$ pc (for a Doppler factor $\delta \sim 11$; Lähteenmäki & Valtaoja 1999), which is much larger than the expected size of the VLBI core region (several parsec). This may suggest that suboutburst *H* is associated with the development of a dense region, perhaps some kind of 'cocoon' that confines the innermost part of the jet that is excited by the primary perturbation. However, the observed profile width may also be dependent on the rates of adiabatic and synchrotron losses, which are difficult to estimate with any degree of certainty in the absence of direct VLBI structural information. Therefore, the real size for the excitation region associated with suboutburst *H* must be considered unknown. According to our classification (Paper I), suboutburst *H* is mixed, and exhibits properties of both core (frequency-dependent time delays) and jet (association with ejected jet components) outbursts.

The similarity between the time lags for flares *A*, *B*, *C* and *D* and those for flares *E*, *F*, *G* and *I*, as well as the relatively high flux levels at 14.5, 8 and 4.8 GHz during the local minima in 1981 (see Fig. 2), suggest that the first outburst contains a prolonged suboutburst similar to event *H* that began somewhat before 1978. However, the lack of data before 1978 prevents us from determining the parameters of this proposed outburst. However, 5 GHz VLBI observations obtained in 1987 April by Gabuzda et al. (1993) reveal a bright component, *K*1, at a distance of $\sim$3.9 mas from the core in PA$\sim -86^\circ$. If this component moved with the typical proper motion observed in the jet of this blazar, $\sim$0.3 mas yr^{-1} (Kellermann et al. 2004), then it should have been ejected near 1975. This date could be associated with the onset of the first outburst, which would then last from 1975 to 1988 and have a similar duration as the second outburst in 1988–2001, $\sim$14 yr. This duration is only approximate, and may represent a lower limit for the duration of the activity cycle of this source due to the large uncertainty in the epoch of the onset of the first cycle. The flares at different frequencies for the same event have similar profiles, although Θ differs from flare to flare and from cycle to cycle. This variation in Θ defines the fine structure of an outburst, and may reflect interaction between the primary perturbation and inhomogeneities in the jet and/or external medium (Marscher, Travis & Gear 1992; Gómez et al. 2000). However, the Θ for suboutburst *H*, which we have suggested is associated with the primary

Table 2. 2223-052: parameters of outbursts.

Comp.	Freq. (GHz)	Amplitude (Jy)	T_{max} (yr)	Θ (yr)	Time delay (yr)	σ^2
A1	36.8	8.65 ± 0.27	1983.80 ± 0.08	2.27 ± 0.05	0.00 ± 0.08	1.84
A1	22.2	6.66 ± 0.33	1983.71 ± 0.04	2.36 ± 0.04	-0.09 ± 0.09	0.57
A1	14.5	5.90 ± 0.02	1984.15 ± 0.01	1.65 ± 0.01	0.35 ± 0.09	0.12
A1	8.0	4.48 ± 0.02	1984.37 ± 0.01	1.66 ± 0.01	0.57 ± 0.09	0.12
A1	4.8	2.13 ± 0.04	1984.74 ± 0.02	1.88 ± 0.02	0.94 ± 0.09	0.05
B1a	36.8	5.33 ± 0.05	1988.87 ± 0.05	3.80 ± 0.05	0.00 ± 0.05	0.36
B1a	22.2	3.94 ± 0.10	1988.85 ± 0.08	2.80 ± 0.07	-0.02 ± 0.09	0.21
B1a	14.5	3.45 ± 0.02	1989.23 ± 0.02	3.01 ± 0.02	0.37 ± 0.05	0.17
B1a	8.0	2.58 ± 0.02	1989.65 ± 0.04	3.89 ± 0.03	0.78 ± 0.06	0.04
B1a	4.8	1.49 ± 0.01	1989.51 ± 0.06	3.09 ± 0.08	0.64 ± 0.08	0.02
B1b	36.8	4.17 ± 0.08	1990.35 ± 0.01	0.95 ± 0.01	0.00 ± 0.01	0.26
B1b	22.2	4.74 ± 0.12	1990.46 ± 0.02	1.12 ± 0.02	0.11 ± 0.02	0.30
B1b	14.5	2.58 ± 0.03	1990.43 ± 0.01	0.74 ± 0.01	0.08 ± 0.02	0.11
B1b	8.0	1.62 ± 0.04	1990.56 ± 0.01	0.71 ± 0.01	0.21 ± 0.02	0.06
B1b	4.8	0.85 ± 0.02	1990.64 ± 0.01	0.72 ± 0.01	0.29 ± 0.02	0.02
B1c	36.8	1.43 ± 0.05	1991.78 ± 0.02	1.07 ± 0.02	0.00 ± 0.02	0.10
B1c	22.2	2.04 ± 0.08	1992.00 ± 0.03	1.41 ± 0.02	0.22 ± 0.04	0.18
B1c	14.5	2.07 ± 0.01	1991.83 ± 0.01	1.95 ± 0.02	0.05 ± 0.03	0.03
B1c	8.0	1.58 ± 0.02	1992.46 ± 0.02	2.01 ± 0.02	0.68 ± 0.03	0.04
B1c	4.8	1.65 ± 0.01	1992.51 ± 0.02	2.72 ± 0.02	0.73 ± 0.03	0.02
A2	36.8	2.40 ± 0.07	1996.35 ± 0.02	1.91 ± 0.02	0.00 ± 0.02	0.16
A2	22.2	2.43 ± 0.05	1996.56 ± 0.02	1.87 ± 0.02	0.21 ± 0.03	0.11
A2	14.5	2.24 ± 0.02	1996.88 ± 0.01	1.87 ± 0.01	0.53 ± 0.03	0.05
A2	8.0	0.56 ± 0.02	1997.13 ± 0.03	1.71 ± 0.03	0.78 ± 0.04	0.02
B2	36.8	5.14 ± 0.06	2000.74 ± 0.02	3.63 ± 0.02	0.00 ± 0.02	0.48
B2	22.2	6.32 ± 0.08	2000.76 ± 0.02	3.59 ± 0.02	0.02 ± 0.03	0.14
B2	8.0	4.01 ± 0.01	2001.34 ± 0.01	3.75 ± 0.01	0.60 ± 0.03	0.09
B2	4.8	2.88 ± 0.01	2001.81 ± 0.01	3.65 ± 0.01	1.07 ± 0.03	0.05

perturbation, decreases at lower frequencies. This is unexpected, since the durations of flares in blazars are usually shorter at higher frequencies. One possibility is that this is associated with acceleration or bending of the jet flow, such that the Doppler factor increases with distance down the jet within the region where the jet remains optically thick at lower frequencies. Such acceleration could also explain the very high apparent speeds found for some components in the jet, ∼23 c (Lister 2005), which is higher than the average apparent speed reported for EGRET quasars at 15 GHz (Kellermann et al. 2004), which display the fastest bulk Lorentz factors among extragalactic radio sources (Jorstad et al. 2001).

As we can see in Fig. 2, the total 37 GHz flux density increases after 2001.5, possibly indicating the onset of a new activity cycle. The Radio Reference Frame Image Data base (Fey et al. 2005) provides support for this interpretation: the 43 GHz images show an increase in the core flux density, from 1.03, to 1.6, to 2.9 Jy beam^{-1} at epochs 2001.65, 2002.37 and 2003.70, respectively.

4 2223−052 (3C 446)

Like 1308+326, 2223−052 ($z = 1.404$) has intermediate properties between those of quasars and BL Lac objects, displaying prominent broad emission lines (typical for quasars) during its quiescent state and high linear polarization and a strong, featureless continuum (typical for BL Lac objects) in its active state (Barbieri et al. 1985). Multifrequency radio light curves covering 1980 to 2004 are shown in Fig. 4. In addition to the UMRAO and MRO data, these contain 33.5 GHz data of Flett & Henderson (1981, 1983) and 36.8 and 22 GHz data of Salonen et al. (1987). We determined the long-term trends via a linear interpolation across the local/global minima in 1981, 1986, 1994 and 2004. The parameters of the Gaussian components used to decompose the outbursts are presented in Table 2.

A time series analysis of the light curves performed by Kudryavtseva & Pyatunina (2006) identified the presence of two periods in the data: $P_1 = 10.9 \pm 0.2$ yr and $P_2 = 5.8 \pm 0.5$ yr. As we can see from Fig. 4, the shorter period characterizes the average interval between the maxima of prominent outbursts, while the longer period reflects similarities in the shapes of the outbursts. Each long cycle starts with an isolated outburst (*A*1 in 1984 and *A*2 in 1996), which are followed by prolonged, multicomponent suboutbursts. Unfortunately, the parameters of *A*1 at 37 and 22 GHz are affected by the small number of data points at the high frequencies prior to 1986.

Fig. 5 shows the amplitudes and time lags of all components as functions of frequency. The amplitude spectra of the outburst *A*1 and flares *B*1*a* and *B*1*b* are dominated by high-frequency components. The low-frequency delay of outburst *A*1 is ∼0.9 yr, while the flares *B*1*a* and *B*1*b* display the moderate delay of $\Delta T \sim 0.6$ yr. The time lag for the flare *B*1*c* increases to $\Delta T \sim 1.0$ yr, accompanied by flattening of the spectrum. This evolution suggests that *B*1*a*, *B*1*b* and *B*1*c* represent the fine structure of a single event, *B*1. The low-frequency delay and steep amplitude spectrum of the outburst *A*2 are similar to those observed for *A*1. Suboutburst *B*2 has a long time-lag ($\Delta T \sim 1.3$ yr) and a flat spectrum, like *B*1*c*. We were not able to decompose the fine structure of suboutburst *B*2, because it has characteristics similar to those of white noise.

Table 3. 2251+158: parameters of outbursts.

Comp.	Freq. (GHz)	Amplitude (Jy)	T_{max} (yr)	Θ (yr)	Time delay (yr)	σ^2
A2	36.8	7.22 ± 0.21	1981.81 ± 0.02	0.97 ± 0.03	0.00 ± 0.02	1.13
A2	22.2	8.97 ± 0.17	1981.74 ± 0.03	1.06 ± 0.02	-0.07 ± 0.04	0.49
A2	14.5	11.44 ± 0.03	1981.86 ± 0.02	0.82 ± 0.01	0.05 ± 0.03	0.34
A2	8.0	11.23 ± 0.02	1982.19 ± 0.01	1.16 ± 0.01	0.38 ± 0.03	0.11
A2	4.8	8.45 ± 0.03	1982.70 ± 0.01	1.15 ± 0.01	0.89 ± 0.03	0.12
B2	22.2	1.68 ± 0.09	1985.04 ± 0.02	0.33 ± 0.02	0.00 ± 0.02	0.27
B2	14.5	1.80 ± 0.02	1985.11 ± 0.01	0.65 ± 0.01	0.07 ± 0.03	0.14
B2	8.0	1.74 ± 0.02	1985.06 ± 0.01	0.62 ± 0.01	0.02 ± 0.03	0.09
B2	4.8	1.54 ± 0.05	1984.97 ± 0.02	0.49 ± 0.02	-0.07 ± 0.03	0.10
C2	36.8	3.85 ± 0.05	1987.20 ± 0.02	0.72 ± 0.03	0.00 ± 0.02	0.56
C2	22.2	4.38 ± 0.06	1987.11 ± 0.03	1.03 ± 0.04	-0.09 ± 0.04	0.39
C2	14.5	5.46 ± 0.02	1987.38 ± 0.01	1.35 ± 0.01	0.18 ± 0.03	0.21
C2	8.0	6.80 ± 0.02	1987.48 ± 0.01	1.32 ± 0.01	0.28 ± 0.03	0.14
C2	4.8	6.27 ± 0.02	1987.78 ± 0.01	1.41 ± 0.02	0.58 ± 0.03	0.14
D2	36.8	6.13 ± 0.05	1989.03 ± 0.01	0.45 ± 0.01	0.00 ± 0.01	0.49
D2	22.2	4.97 ± 0.08	1989.19 ± 0.01	0.56 ± 0.01	0.16 ± 0.02	0.25
D2	14.5	4.18 ± 0.03	1989.41 ± 0.01	0.42 ± 0.01	0.38 ± 0.02	0.11
D2	8.0	3.70 ± 0.03	1989.56 ± 0.01	0.47 ± 0.01	0.53 ± 0.02	0.07
D2	4.8	2.42 ± 0.03	1989.76 ± 0.01	0.62 ± 0.01	0.73 ± 0.02	0.14
A3	90.0	7.14 ± 0.23	1990.86 ± 0.01	0.60 ± 0.01	–	1.39
A3	36.8	4.19 ± 0.05	1990.97 ± 0.02	0.47 ± 0.02	0.00 ± 0.02	0.19
A3	22.2	1.98 ± 0.07	1991.08 ± 0.03	0.64 ± 0.02	0.11 ± 0.04	0.11
A3	14.5	0.83 ± 0.03	1991.28 ± 0.01	0.48 ± 0.01	0.31 ± 0.03	0.03
B3	90.0	3.69 ± 0.12	1991.79 ± 0.01	0.29 ± 0.01	–	0.36
B3	36.8	3.28 ± 0.11	1991.84 ± 0.02	0.31 ± 0.01	0.00 ± 0.02	0.07
B3	22.2	3.39 ± 0.08	1991.99 ± 0.01	0.35 ± 0.01	0.15 ± 0.03	0.18
B3	14.5	4.08 ± 0.03	1992.42 ± 0.01	0.45 ± 0.01	0.58 ± 0.03	0.07
B3	8.0	1.68 ± 0.05	1992.46 ± 0.01	0.41 ± 0.01	0.62 ± 0.03	0.09
C3	36.8	4.23 ± 0.07	1992.14 ± 0.02	0.29 ± 0.02	0.00 ± 0.02	0.09
C3	22.2	5.73 ± 0.17	1992.39 ± 0.01	0.40 ± 0.02	0.25 ± 0.03	0.44
C3	14.5	4.62 ± 0.04	1992.86 ± 0.02	0.40 ± 0.01	0.72 ± 0.03	0.27
C3	8.0	3.37 ± 0.05	1992.97 ± 0.01	0.57 ± 0.01	0.83 ± 0.03	0.08
B3+C3	4.8	1.28 ± 0.02	1992.86 ± 0.01	0.52 ± 0.02	0.72 ± 0.03	0.03
D3	90.0	5.74 ± 0.11	1992.54 ± 0.01	0.71 ± 0.01	–	0.57
D3	36.8	6.03 ± 0.07	1992.53 ± 0.01	0.46 ± 0.01	0.00 ± 0.01	0.19
D3	22.2	5.32 ± 0.14	1992.83 ± 0.01	0.40 ± 0.01	0.30 ± 0.02	0.30
D3	14.5	6.19 ± 0.08	1993.33 ± 0.01	0.47 ± 0.01	0.80 ± 0.02	0.89
D3	8.0	5.11 ± 0.10	1993.46 ± 0.01	0.30 ± 0.01	0.93 ± 0.02	0.49
D3	4.8	3.33 ± 0.03	1993.54 ± 0.01	0.45 ± 0.01	1.01 ± 0.02	0.05
E3	90.0	7.02 ± 0.91	1993.16 ± 0.01	0.29 ± 0.01	–	0.83
E3	36.8	6.41 ± 0.08	1993.12 ± 0.01	0.55 ± 0.01	0.00 ± 0.01	0.82
E3	22.2	5.40 ± 0.14	1993.24 ± 0.01	0.39 ± 0.01	0.12 ± 0.01	0.76
E3	14.5	6.57 ± 0.07	1993.81 ± 0.01	0.48 ± 0.01	0.69 ± 0.02	0.63
E3	8.0	5.26 ± 0.07	1993.84 ± 0.01	0.43 ± 0.01	0.72 ± 0.02	0.19
E3	4.8	2.39 ± 0.05	1993.98 ± 0.01	0.38 ± 0.01	0.86 ± 0.02	0.13
F3	90.0	9.32 ± 0.23	1994.15 ± 0.01	1.15 ± 0.02	–	1.52
F3	36.8	10.72 ± 0.10	1994.11 ± 0.02	0.95 ± 0.02	0.00 ± 0.02	0.48
F3	22.2	11.20 ± 0.13	1994.25 ± 0.01	1.29 ± 0.01	0.14 ± 0.03	0.34
F3	14.5	12.74 ± 0.10	1994.47 ± 0.01	0.80 ± 0.01	0.36 ± 0.03	1.14
F3	8.0	11.23 ± 0.07	1994.55 ± 0.01	1.04 ± 0.01	0.44 ± 0.03	0.42
F3	4.8	7.85 ± 0.05	1994.68 ± 0.01	1.10 ± 0.01	0.57 ± 0.03	0.18
G3+H3	36.8	5.71 ± 0.05	1995.31 ± 0.01	0.91 ± 0.01	0.00 ± 0.01	0.27
G3	22.2	5.41 ± 0.08	1995.41 ± 0.01	0.51 ± 0.01	0.10 ± 0.02	0.15
G3+H3	14.5	6.39 ± 0.10	1995.55 ± 0.01	0.83 ± 0.02	0.24 ± 0.02	0.43
G3+H3	8.0	4.09 ± 0.09	1995.58 ± 0.01	0.58 ± 0.01	0.27 ± 0.02	0.08
G3+H3	4.8	3.45 ± 0.04	1995.74 ± 0.01	0.74 ± 0.01	0.43 ± 0.02	0.10
I3+J3	36.8	3.46 ± 0.07	1996.45 ± 0.02	0.80 ± 0.02	0.00 ± 0.02	0.20
I3	22.2	4.42 ± 0.77	1996.20 ± 0.08	0.48 ± 0.04	-0.25 ± 0.08	0.09
I3+J3	14.5	5.04 ± 0.04	1996.54 ± 0.01	0.71 ± 0.02	0.11 ± 0.03	0.43
I3+J3	8.0	6.14 ± 0.04	1996.42 ± 0.01	1.11 ± 0.02	-0.03 ± 0.03	0.14
I3+J3	4.8	5.61 ± 0.05	1996.54 ± 0.01	0.83 ± 0.03	0.09 ± 0.03	0.27

Table 3 – *continued*

Comp.	Freq. (GHz)	Amplitude (Jy)	T_{max} (yr)	Θ (yr)	Time delay (yr)	σ^2
K3	36.8	2.36 ± 0.05	1997.21 ± 0.01	0.70 ± 0.01	0.00 ± 0.01	0.17
K3	22.2	3.21 ± 0.05	1997.21 ± 0.01	0.59 ± 0.01	0.00 ± 0.01	0.14
K3	14.5	3.01 ± 0.07	1997.42 ± 0.01	0.50 ± 0.03	0.21 ± 0.01	0.15
K3	8.0	2.63 ± 0.07	1997.51 ± 0.01	0.68 ± 0.03	0.30 ± 0.01	0.06
K3	4.8	2.87 ± 0.04	1997.63 ± 0.01	0.85 ± 0.01	0.42 ± 0.01	0.33
M3	36.8	3.33 ± 0.08	1998.64 ± 0.01	0.93 ± 0.01	0.00 ± 0.01	0.07
M3	22.2	5.11 ± 0.09	1998.52 ± 0.02	0.42 ± 0.01	-0.12 ± 0.02	0.13
M3	14.5	3.72 ± 0.03	1998.56 ± 0.01	0.83 ± 0.01	-0.08 ± 0.01	0.10
M3	8.0	3.55 ± 0.05	1998.57 ± 0.02	0.49 ± 0.04	-0.07 ± 0.02	0.08
M3	4.8	2.54 ± 0.03	1998.63 ± 0.01	0.92 ± 0.02	-0.01 ± 0.01	0.66
P3	36.8	4.59 ± 0.11	2000.20 ± 0.01	0.56 ± 0.01	0.00 ± 0.01	0.29
P3	22.2	3.87 ± 0.06	2000.29 ± 0.01	0.65 ± 0.01	0.09 ± 0.01	0.15
P3	14.5	2.61 ± 0.02	2000.42 ± 0.01	0.55 ± 0.01	0.23 ± 0.01	0.06
P3	8.0	0.87 ± 0.02	2000.59 ± 0.01	0.49 ± 0.01	0.39 ± 0.01	0.08
P3	4.8	0.98 ± 0.03	2000.70 ± 0.02	0.49 ± 0.01	0.50 ± 0.02	0.11
Q3	36.8	3.40 ± 0.09	2001.43 ± 0.01	0.50 ± 0.02	0.00 ± 0.01	0.11
Q3	22.2	3.26 ± 0.16	2001.45 ± 0.02	0.50 ± 0.03	0.02 ± 0.02	0.07
Q3	14.5	2.99 ± 0.03	2001.43 ± 0.01	0.55 ± 0.01	0.00 ± 0.01	0.14
Q3	8.0	1.99 ± 0.04	2001.38 ± 0.01	0.50 ± 0.01	-0.05 ± 0.01	0.08
Q3	4.8	1.49 ± 0.03	2001.43 ± 0.01	0.77 ± 0.01	0.00 ± 0.01	0.11
R3	36.8	1.75 ± 0.07	2001.92 ± 0.01	0.26 ± 0.01	0.00 ± 0.01	0.07
R3	22.2	1.19 ± 0.07	2002.01 ± 0.02	0.45 ± 0.02	0.09 ± 0.02	0.07
R3	14.5	1.36 ± 0.05	2001.96 ± 0.01	0.29 ± 0.01	0.04 ± 0.01	0.07
R3	8.0	0.97 ± 0.06	2001.98 ± 0.01	0.23 ± 0.01	0.06 ± 0.01	0.13

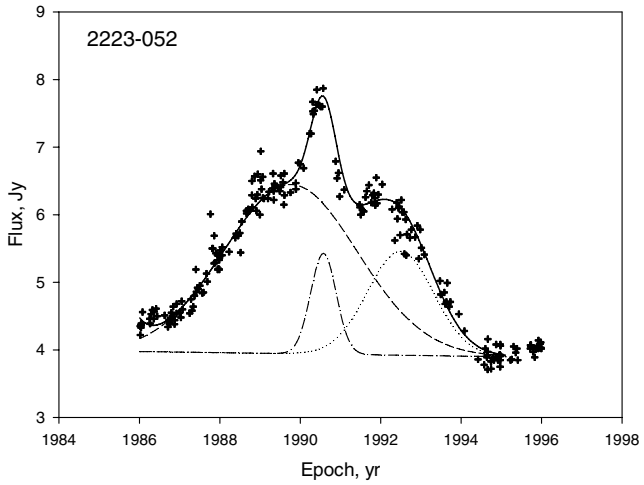

Figure 1. Example of decomposition of an outburst into Gaussian components. Shown is outburst *B*1 (solid curve) in 2223−052 at 14.5 GHz, which has been decomposed into the components *B*1*a* (dashed), *B*1*b* (dash–dotted) and *B*1*c* (dotted).

The VLBI data for 2223−052 prior to 1995 are sparse: the only high-resolution image referring this time is that of Lerner et al. (1993), obtained at 100 GHz in 1990 April. This map reveals a compact, nearly unresolved core and a fairly strong component ∼100 μ*as* to the southwest. This component could plausibly have been ejected in the beginning of 1990, in which case it could be associated with the flare *B*1*b*. Since 1995, the source has been observed more regularly as part of the 15 GHz multi-epoch VLBA program of Kellermann et al. (1998, 2004). These data reveal new jet components ejected in 1981.4 ± 1.6 and 1994.0 ± 0.8. Given the large uncertainties in the ejection times, the first component may be associated with outburst *A*1 and the second with *A*2. Recent results from the Monitoring of Jets in Active galactic nuclei with VLPA (MOJAVE) 15-GHz survey (Lister 2005) indicate that another new component was ejected prior to 2001. This knot is probably associated with the complex outburst *B*2. According to our classification, all the outbursts show mixed properties. However, the *A* outbursts have a steep amplitude spectrum (the amplitude of the Gaussian component versus frequency), similar to that expected when a flux decrease is dominated by adiabatic expansion (Hughes, Aller & Aller 1985), while the *B* outbursts have a flat amplitude spectrum and longer low-frequency time delays, consistent with synchrotron losses being responsible for the electron-energy distribution (Marscher & Gear 1985). This may suggest that the *A* outbursts represent minor perturbations, e.g. associated with shocks formed during interactions between the jet and external medium ('jet' events), while the *B* outbursts correspond to primary perturbations due to the activity in the central engine ('core' events). If this is the case, this blazar may display an activity cycle corresponding to the time interval between successive *B* outbursts, or ∼12 yr, although this possibility must be verified by further monitoring.

5 2251+158 (3C 454.3)

The quasar 2251+158 ($z = 0.859$) is one of relatively few sources that exhibits correlated behaviour at optical and radio wavelengths. Cheng-yue (2001) found a period of ∼12.4 yr using an optical historical light curve covering about 100 yr. Ciaramella et al. (2004) identified a period of 6.3 ± 0.2 yr using radio data from the UMRAO and MRO data bases, or roughly half the period found by Cheng-yue (2001). Kudryavtseva & Pyatunina (2006) show that both periodic components are present in the UMRAO and MRO radio light curves, with $P_1 = (12.4 \pm 0.6)$ and $P_2 = (6.2 \pm 0.1)$ yr.

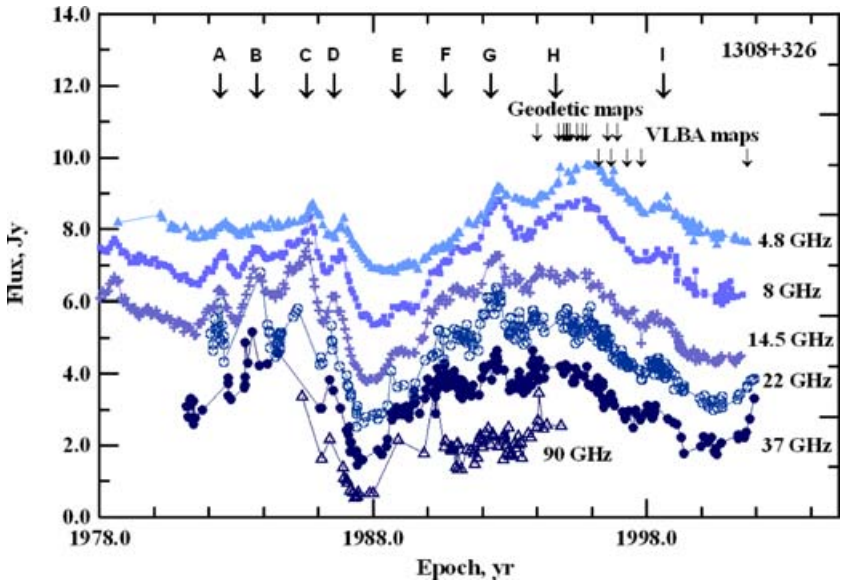

Figure 2. Light curves for 1308+326 at 4.8 GHz (filled triangles), 8 GHz (filled squares), 14.5 GHz (crosses), 22 GHz (open circles), 37 GHz (filled circles) and 90 GHz (open triangles). The light curves have been shifted upwards by 6, 4.5, 3, 2, 1 and 0 Jy, respectively.

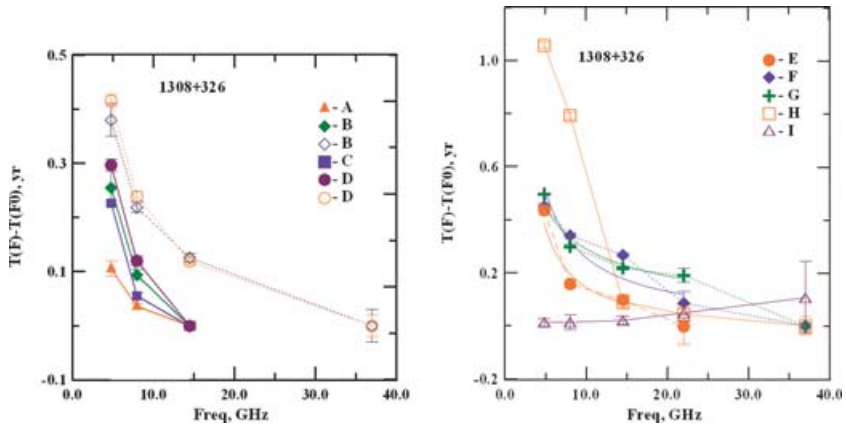

Figure 3. Time delay as a function of frequency for the first (left-hand panel) and second (right-hand panel) outbursts in 1308+326.

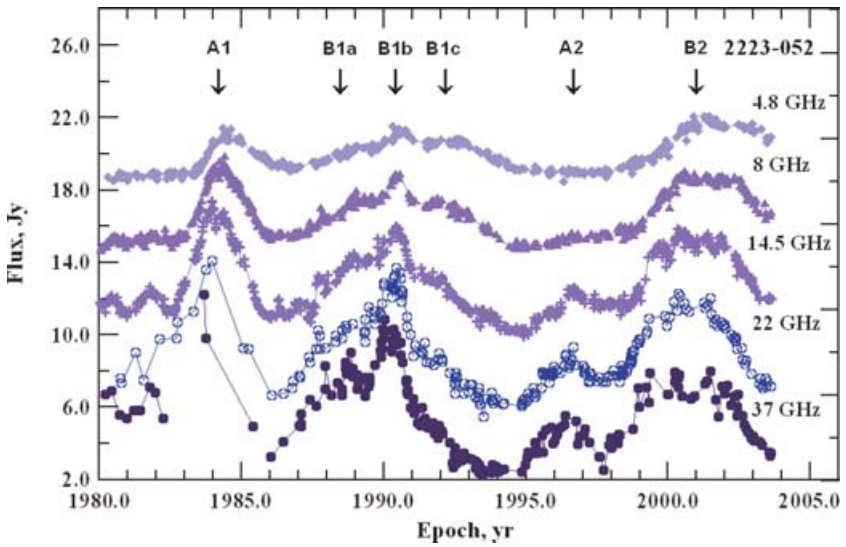

Figure 4. Light curves of 2223−052 at 4.8 GHz (filled boxes), 8 GHz (filled triangles), 14.5 GHz (crosses), 22 GHz (open circles) and 37 GHz (filled circles). The light curves have been shifted upward by 15, 11, 7, 3 and 0 Jy, respectively.

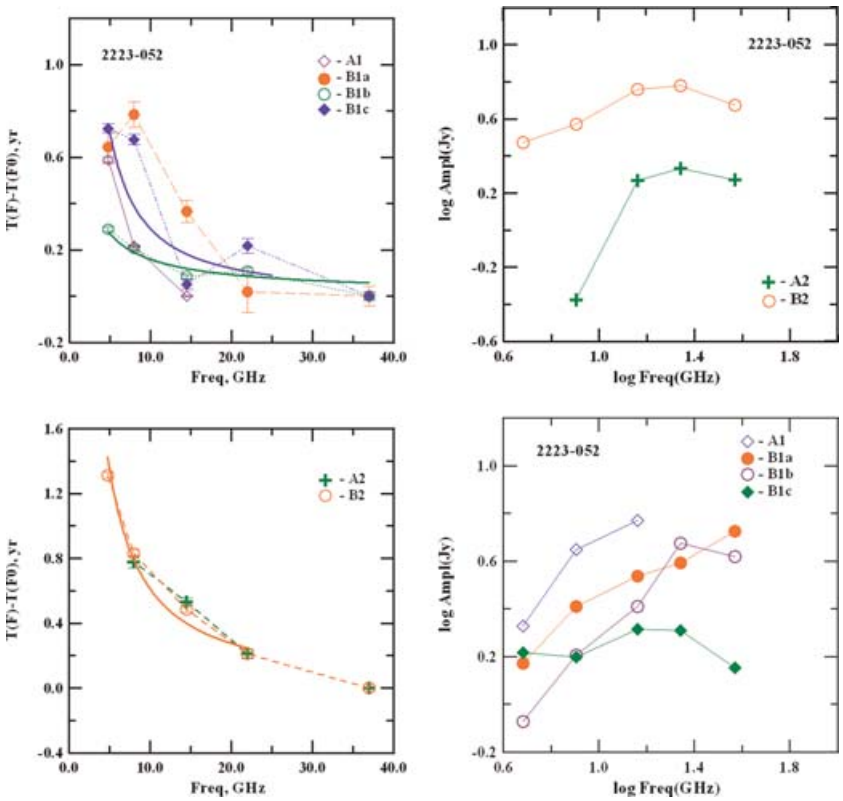

Figure 5. Time delay (left-hand panel) and amplitude (right-hand panel) of individual events as functions of frequency for the first (top) and second (bottom) cycles in 2223−052.

Fig. 6 (top) presents the light curves at 14.5 GHz (the UMRAO data base and Dent, Kapitzky & Kojoian 1974) and at 8 GHz (UMRAO data base). They cover a time interval of ∼40 yr and show three prominent events with maxima in 1968, 1982 and 1994, each followed by less powerful multicomponent flares. Multifrequency light curves at frequencies from 4.8 to 90 GHz are given in Fig. 6 (bottom). The 14.5, 8 and 4.8 GHz data are from the UMRAO, the 22 and 37 GHz points are from the MRO and 90 GHz flux densities are from the IRAM data of Steppe et al. (1988, 1992, 1993) and Reuter et al. (1997).

A visual inspection of Fig. 6 confirms the presence of a ∼12 yr cycle in the radio variability, as was indicated earlier by the time series analysis. We took the beginning of the first cycle to be in 1966, in accordance with the shape of the prominent outburst in 1968. The second cycle starts in 1978.4, and the third cycle begins in 1990.8. The beginning of a cycle is defined by the high-frequency observations, and depends slightly on frequency. This produces the same delay (∼2 yr) for the peak of the most prominent event in each cycle relative to its onset. Table 3 lists the Gaussian parameters of the individual outbursts for cycles 2 and 3, while Fig. 7 shows the time lags and amplitudes of the outbursts as functions of frequency. An activity cycle starts with outbursts with moderate time lags ($\Delta T \leqslant 0.6$ yr), which are dominated by high-frequency components and show steep amplitude spectra (e.g. *A*3 and *B*3). The delay reaches its maximum value (∼1 yr) for outbursts *A*2 and *D*3 in Cycles 2 and 3, respectively, and then gradually decreases. Near the second half of a cycle, outbursts with maxima simultaneous at all frequencies are observed (*B*2, *I*3 and *M*3).

The evolution of the time lag and amplitude at 37 GHz for consecutive outbursts in Cycle 3 is presented in Fig. 8, which shows that the time lag and amplitude increase as a cycle proceeds, reaching their maximum values during the first half of the cycle. The peak time lags occur ∼1.5 yr before the peak amplitudes. This can easily be understood if the outbursts are associated with shocks in the innermost part of the jet. In this case, the maximum time lag corresponds to the maximum optical depth of the shocked region, while the maximum amplitude corresponds to the region where the optical depth becomes equal to unity, and the region becomes transparent at a given frequency.

VLBI observations of the quasar obtained at 10.6 GHz at nine epochs between 1981.4 and 1985.9 (Pauliny-Toth et al. 1984, 1987) show dramatic changes in the jet structure and the appearance of superluminal components with high apparent speeds between 1982.1 and 1983.8 in PA $\sim -95^\circ$. These can confidently be associated with outburst *A*2. Therefore, the low-frequency-delay outburst *A*2 is accompanied by the ejection of superluminal components, and so can be classified as a mixed outburst. The maxima of the next outburst, *B*2, are almost simultaneous at all frequencies. The parsec-scale jet of 2251+158 contains a quasi-stationary feature, *C*, ∼ 0.7 mas from the core in PA $\sim -90^\circ$ (e.g. Gómez, Marscher & Alberdi 1999). The most prominent superluminal component ejected near 1982–1983 had a proper motion of ∼0.35 mas yr^{-1} (Pauliny-Toth et al. 1987), implying that the component should have reached the stationary feature near 1984–1985. This epoch coincides with the peaks of outburst *B*2, suggesting we should classify *B*2 as a jet outburst that is associated with an interaction between moving and stationary shocks in the jet. The only VLBI data available during outbursts *C*2 and *D*2 are the 5-GHz data for epoch 1988.2 of Cawthorne & Gabuzda (1996). The polarization structure of the source led these authors to conclude that 2251+158 may have been in the process of giving birth to a new jet component at the epoch of their observation. In this case, this component could be associated with outburst

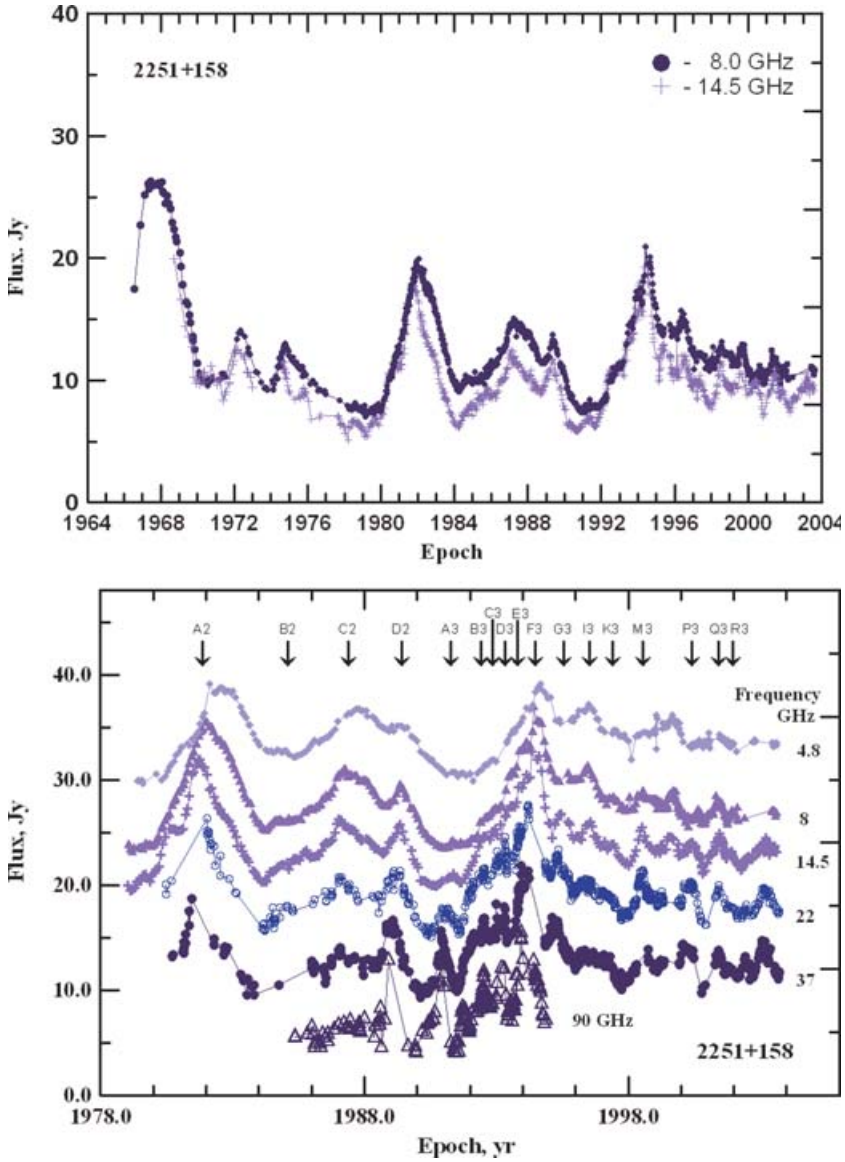

Figure 6. Top: master light curves of 2251+158 at 8 and 14.5 GHz. Bottom: light curves at 4.8 GHz (filled diamonds), 8 GHz (filled triangles), 14.5 GHz (crosses), 22 GHz (open circles), 37 GHz (filled circles) and 90 GHz (open triangles). The light curves have been shifted upwards by 22, 16, 14, 10, 5 and 0 Jy, respectively.

*D*2. Though outburst *D*2 exhibits a significant low-frequency delay, its steep amplitude spectrum and the possible connection with a jet component lead us to classify it as a mixed outburst associated with the evolution of the jet. Outburst *C*2 has moderate time lags and a spectrum dominated by a low-frequency component, and may be associated with reverse shocks behind the primary perturbation that partially affect the core region.

Fig. 9 presents the 37 GHz light curve together with the light curves of individual VLBI components ejected from 1994 to 2001 (Jorstad et al. 2001, 2005). The ejection of knots B1 and B2 occurs within ΔT of $T_{\rm max}$(37 GHz) for the brightest outburst *F*3. Therefore, the outburst has the same properties as the most prominent outburst *A*2 in Cycle 2. The much weaker knots B3, B4 and B6 can be associated with outbursts *G*3, *M*3 and *P*3, respectively. The synchronous outburst *M*3 is a pure jet outburst. Another synchronous outburst, *I*3, may be associated with the interaction of knots B1 and/or B2 with the stationary feature C, as was the case for outburst *B*2 in Cycle 2. Although outbursts *G*3 and *P*3 show low-frequency delays, ΔT is moderate. These mixed outbursts are more likely associated with the evolution of the jet than with activity of the central engine. The outburst *K*3 is very similar to *G*3 and *P*3, although it is not accompanied by a jet component. Therefore, each cycle contains an outburst that is strongest, and has the flattest amplitude spectrum and a significant low-frequency time delay: *A*2 in Cycle 2 and *F*3 in Cycle 3. We associate these outbursts with activity of the central engine, and define the duration of the activity cycle to be $T^{F3}_{\rm max} - T^{A2}_{\rm max}$ at 37 GHz: 12.30 ± 0.04 yr. It is especially noteworthy that this period predicted the onset of a new cycle in 2003 and a dramatic increase in the high-frequency flux density in 2005.5, as has now been observed (Villata et al. 2007). The cycle is also consistent with the period $P_1 = (12.4 \pm 0.6)$ yr obtained via time series analysis (Kudryavtseva & Pyatunina 2006). We adopt this latter period as the duration of the activity cycle of the quasar, given the uncertainties in the beginning and end of each cycle.

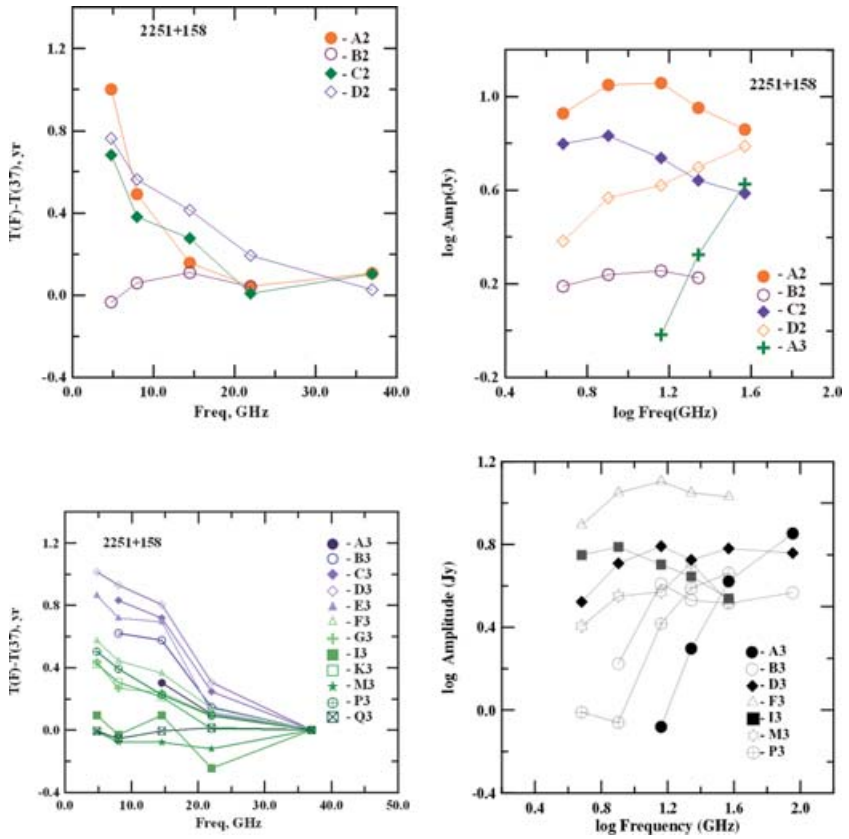

Figure 7. Time delays (left-hand panel) and amplitudes (right-hand panel) of individual events as functions of frequency for the second (top) and third (bottom) cycles in 2251+158.

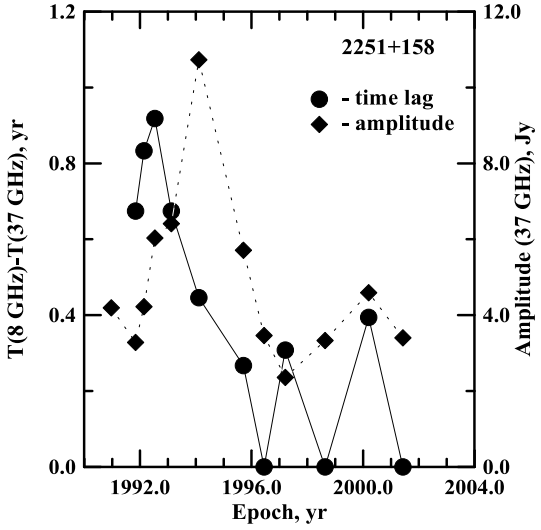

Figure 8. Amplitude at 37 GHz and time lags of individual outbursts as functions of time during Cycle 3 in 2251+158.

6 DISCUSSION

Our results from this paper and Paper I suggest that its activity cycle is one of the defining characteristics of a blazar, along with other physical parameters, such as the mass and spin of the black hole, accretion rate, Lorentz and Doppler factors and magnetic-field strength. For some sources, the long-term data accumulated to date are sufficient to determine the duration of the activity cycle, while for others only a lower limit can be estimated. However, it appears that, for all the blazars we have studied, an activity cycle includes a major event with frequency stratification at radio wavelengths, accompanied by the ejection of one or more jet components. This event occupies only a fraction of the cycle. This behaviour is qualitatively consistent with the sustenance model of a black hole suggested by Shields & Wheeler (1978), in which an active nucleus stores infalling mass during a quiescent period in the accretion disc, and then releases this mass through instability over a shorter period of intensive activity. This scenario might be observed in black hole binary systems where a low/hard state of the X-ray emission can be associated with a quiescent period and a high/soft state with an active period (Fender & Belloni 2004). The transition from the low-to-high state is accompanied by the appearance of a highly relativistic radio jet. In our blazars, a major event corresponds to a period of intense activity, while a quiescent period is quiescent only for the central engine, since the jet can remain active. This model does not require cycles to be strictly periodic, since a cycle can depend on many parameters, such as the accretion rate or stored mass before an instability is triggered, which might differ from cycle to cycle.

Table 4 gives the activity cycle, $T_{\rm act}$, typical time-scale, $\Theta_{\rm maj}$, and amplitude, $A_{\rm maj}$, of the major event in each cycle for the sources studied in this paper, Paper I and Pyatunina et al. (2000, 2003, 2005). The parameter $\Theta_{\rm maj}$ is the FWHM of the Gaussian component corresponding to the outburst that shows the most significant low-frequency delay, while $A_{\rm maj}$ is the amplitude of this Gaussian (FWHM and $A_{\rm maj}$ are determined at 14.5 GHz). Table 4 also

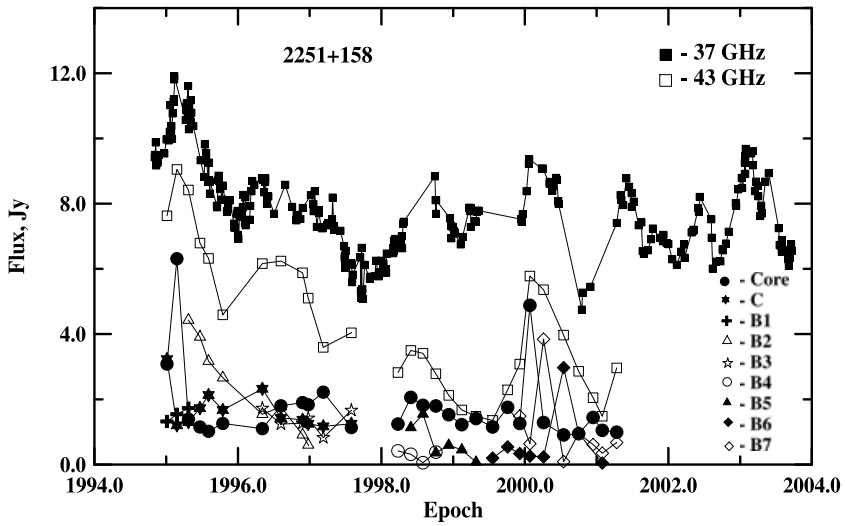

Figure 9. 37 GHz light curve (filled squares) and flux densities of VLBI components at 43 GHz located within 0.6 mas of the core in 2251+158 (the open squares represent the sum of all components).

Table 4. Characteristics of activity cycles.

Source	z	δ	$T_{\rm act}$ (yr)	$\Theta_{\rm maj}$ (yr)	$A_{\rm maj}$ (Jy)	S_q (Jy)
0059+581	0.643	4.7[a]	4.5	1.2	1.8	1.0
0133+476	0.859	7.1	$\geqslant$12			1.5
0202+149	0.833	5.9	4	1.0	1.5	2.0
0458−020	2.27	17.8	$\geqslant$16	2.7	2.5	1.5
0528+134	2.06	14.2	14	1.6	7.3	2.5
0945+408	1.25	10.1	$\geqslant$25	2.4	0.9	1.0
1308+326	0.996	11.4	$\geqslant$14	5.8	3.0	2.0
1730−130	0.90	11.2	$\geqslant$9	2.1	10.1	4.0
2223−052	1.404	11.4	12	4.1	5.7	4.0
2230+114	1.04	14.2	8.0 ± 0.3	0.7	2.1	2.5
2251+158	0.859	21.8	12.4 ± 0.6	0.8	11.4	6.0

[a]The estimate of δ is based on the apparent speed given by Pyatunina et al. (2003).

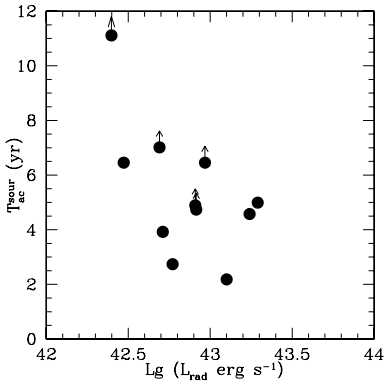

Figure 10. Duration of activity cycle versus radio luminosity.

contains the redshift, z, Doppler factor, δ ($D_{\rm var}$ from Lähteenmäki & Valtaoja 1999) and the quiescent radio flux density derived from the long-term trend at 14.5 GHz, S_q. Despite the small size of the sample, some preliminary results can be obtained. We calculated the radio luminosities of the sources in their quiescent states in their rest frames, $L_{\rm rad} = 4\pi D_{\rm L}^2 S_q/(1+z)/\delta^2$, where $D_{\rm L}$ is the luminosity distance. A plot of the activity-cycle durations in the source frames, $T^{\rm sour}_{\rm act} = T_{\rm act}/(1+z)$, versus this luminosity is shown in Fig. 10. We might expect that more powerful radio sources should have longer activity cycles, corresponding to larger masses and size scales. However, Fig. 10 suggests the opposite tendency: more luminous blazars appear to have shorter activity cycles and experience major events more frequently. We have calculated a partial linear correlation coefficient between $L_{\rm rad}$ and $T^{\rm sour}_{\rm ac}$ as described by Padovani (1992), which enables us to exclude the redshift dependence in the variables. This yields a correlation coefficient of -0.58, which is significant at the level $\alpha = 0.15$, indicating a tentative anticorrelation between $L_{\rm rad}$ and $T^{\rm sour}_{\rm ac}$. We also analysed the relationship between the relative amplitudes of major events ($A_{\rm maj}/S_q$) and their luminosities (linear correlation coefficient 0.16) and between the durations of major events relative to the activity cycle ($T_{\rm maj}/T_{\rm ac}$) and their luminosities (correlation coefficient 0.37). Although these correlation coefficients are not formally statistically significant, they are both positive. This is expected for sustenance models such as that of Shields & Wheeler (1978), where more luminous sources should release larger amounts of additional energy during periods of intensive activity, with these periods of intensive activity occupying a larger fraction of the activity cycle than in less luminous sources. In our sample, the periods of intensive activity can occupy up to half the cycle in the most luminous sources, but do not exceed 10–20 per cent of the cycle in less powerful sources. Of course, all these tentative correlations must be verified based on somewhat larger samples of sources.

In our scenario, in which the radio variability of blazars can be understood in terms of cycles of activity of the central engine, a shorter activity cycle for more luminous blazars implies that they can accrete relatively larger amounts of mass in a given time interval than their less luminous counterparts. This suggests higher accretion rates (in Eddington units) for more powerful sources, which should also lead to the more rapid creation of the conditions required for the growth of instability, given comparable black hole masses. Unfortunately, the masses of the black holes in blazars are poorly known, and this hypothesis must be tested using a larger sample of blazars covering a wider range of luminosities and including sources with estimates for the masses of their central black holes.

7 CONCLUSION

We have analysed multifrequency radio light curves of several blazars jointly with high-resolution VLBA data. Our results can be summarized as follows.

(i) We find that the activity of the central engines in blazars is manifest in their radio light curves by outbursts with flat amplitude spectra and significant low-frequency time lags ('core' events).

(ii) We have determined the activity cycles in 1308+326, 2223−052 and 2251+158 to have durations of $\geqslant$14, $\sim$12 and 12.4 ± 0.6 yr, respectively.

(iii) The structure of the outbursts in 1308+326 suggests an acceleration of the jet flow within the optically thick region, which can explain the very high apparent speeds derived for jet components.

(iv) The evolution of outbursts within individual activity cycles in 2251+158 shows that the outburst displaying the longest low-frequency time-lag precedes the outburst with the highest amplitude, consistent with the shock-in-jet model (e.g. Marscher & Gear 1985).

(v) We have found tentative evidence that more luminous radio sources possess shorter activity cycles, which may suggest higher accretion rates in more powerful AGNs, relative to the Eddington rate.

ACKNOWLEDGMENTS

NAK was supported for this research through a stipend from the International Max-Planck Research School (IMPRS) for Radio and Infrared Astronomy at the Universities of Bonn and Cologne. UMRAO has been supported by a series of grants from the NSF (most recently AST–0307629) and by funds from the University of Michigan. SGJ was partially supported by National Science Foundation grant AST04-06865. The research has made use of the United States Naval Observatory (USNO) Radio Reference Frame Image Data base (RRFID). We also acknowledge data provided by the Metsähovi Radio Observatory, MOJAVE and VLBA 2-cm Survey Program teams.

REFERENCES

Agudo I., Gómez J. L., Gabuzda D. C., Alberdi A., Marscher A. P., Jorstad S. G., 2002, in Ros E., Porcas R. W., Lobanov A. P., Zensus J. A., eds, Proc. 6th European VLBI Network Symposium. Max-Planck-Institut für Radioastronomie, Bonn, p. 15

Aller H. D., Aller M. F., Latimer G. E., Hodge P. E., 1985, ApJS, 59, 513

Aloy M.Á. Martí J.-M., Gómez J.-L., Agudo I., Müller E., Ibáñez J. M., 2003, ApJ, 585, L109

Barbieri C., Omizzolo S., Romano G., Cristiani S., 1985, A&A, 142, 316

Cawthorne T. V., Gabuzda D. C., 1996, MNRAS, 278, 861

Cheng-yue S., 2001, Chin. Astron. &Astrophys., 25, 153

Ciaramella A. et al., 2004, A&A, 419, 485

Dent W. A., Kapitzky J. E., Kojoian G., 1974, AJ, 79, 1232

Fender R., Belloni T., 2004, ARA&A, 42, 317

Fey A. L., Boboltz D. A., Charlot P., Fomalont E. B., Lanyi G. E., Zhang L. D., 2005, in Romney J. D., Reid M. J., eds, ASP Conf. Ser. Vol. 340, Future Directions in High Resolution Astronomy. Astron. Soc. Pac., San Francisco, p. 514

Flett A. M., Henderson C., 1981, MNRAS, 194, 961

Flett A. M., Henderson C., 1983, MNRAS, 204, 1285

Gabuzda D. C., Kollgaard R. I., Roberts D. H., Wardle J. F. C., 1993, ApJ, 410, 39

Gómez J. L., Marscher A. P., Alberdi A., 1999, ApJ, 522, 74

Gómez J. L., Marscher A. P., Alberdi A., Jorstad S. G., Garcia-Miró C., 2000, Sci., 289, 2317

Gómez J. L., Marscher A. P., Alberdi A., Jorstad S. G., Agudo I., 2001, ApJ, 561, 161

Homan D. C., Ojha R., Wardle J. F. C., Roberts D. H., Aller M. F., Aller H. D., Hughes P. A., 2001, ApJ, 549, 840

Hughes P. A., Aller H. D., Aller M. F., 1985, ApJ, 298, 301

Jorstad S. G., Marscher A. P., Mattox J. R., Aller M. F., Aller H. D., Wehrle A. E., Bloom S. D., 2001, ApJ, 556, 738

Jorstad S. G. et al., 2005, AJ, 130, 1418

Kellermann K. I., Vermeulen R. C., Zensus J. A., Cohen M. H., 1998, AJ, 115, 1295

Kellermann K. I. et al., 2004, ApJ, 609, 539

Kidger M. R., 2000, AJ, 119, 2053

Kollgaard R. I., Wardle J. F. C., Roberts D. H., Gabuzda D. C., 1992, AJ, 104, 1687

Kudryavtseva N. A., Pyatunina T. B., 2006, Astron. Rep., 83, 3

Lähteenmäki A., Valtaoja E., 1999, ApJ, 521, 493

Lehto H. J., Valtonen M. J., 1996, ApJ, 460, 207

Lerner M. S. et al., 1993, A&A, 280, 117

Lister M., 2005, in Romney J. D., Reid M. J., eds, ASP Conf. Ser. Vol. 340, Future Directions in High Resolution Astronomy. Astron. Soc. Pac., San Francisco, p. 20

Marscher A. P., Gear W. K., 1985, ApJ, 298, 114

Marscher A. P., Travis J. P., Gear W. K., 1992, in Valtaoja E., Valtonen M., eds, Variability of Blazars. Cambridge Univ. Press, Cambridge, p. 85

Pauliny-Toth I. I. K., Porcas R. W., Zensus J. A., Kellermann K. I., 1984, IAU Symp. 110: VLBI and Compact Radio Sources. Knudsen, p. 149

Pauliny-Toth I. I. K., Porcas R. W., Zensus J. A., Kellermann K. I., Wu S. Y., 1987, Nat, 328, 778

Pursimo T. et al., 2000, A&AS, 146, 141

Pyatunina T. B., Marchenko S. G., Marscher A. P., Aller M. F., Aller H. D., Teräsranta H., Valtaoja E., 2000, A&A, 358, 451

Pyatunina T. B., Rachimov I. A., Zborovskii A. A., Gabuzda D. C., Jorstad S. G., Teräsranta H., Aller M. F., Aller H. D., 2003, in Takalo L. O., Valtaoja E., eds, ASP Conf. Ser. Vol. 299, High Energy Blazar Astronomy. Astron. Soc. Pac., San Francisco, p. 89

Pyatunina T. B., Gabuzda D. C., Jorstad S. G., Aller M. F., Aller H. D., Teräsranta H., 2005, in Romney J. D., Reid M. M., eds, ASP Conf. Ser. Vol. 340, Future Directions in High Resolution Astronomy. Astron. Soc. Pac., San Francisco, p. 198

Pyatunina T. B., Kudravtseva N. A., Gabuzda D. C., Jorstad S. G., Aller M. F., Aller H. D., Teräsranta H., 2006, MNRAS, 373, 1470

Raiteri C. M. et al., 2001, A&A, 377, 396

Reuter H. P. et al., 1997, A&AS, 122, 271

Salonen E. et al., 1987, A&AS, 70, 409

Savolainen T., Wiik K., Valtaoja E., Jorstad S. G., Marscher A. P., 2002, A&A, 394, 851

Shields G. A., Wheeler J. C., 1978, ApJ, 222, 667

Steppe H., Salter C. J., Chini R., Kreysa E., Brunswig W., Lobato-Pérez J., 1988, A&AS, 75, 317

Steppe H., Liechti S., Mauersberger R., Kömpe C., Brunswig W., Ruiz-Moreno M., 1992, A&AS, 96, 441

Steppe H. et al., 1993, A&AS, 102, 611

Stickel M., Fried J. W., Kühr H., Padovani P., Urry C. M., 1991, ApJ, 374, 431

Teräsranta H. et al., 1998, A&AS, 132, 305

Teräsranta H. et al., 2004, A&A, 427, 769

Teräsranta H., Wiren S K. P., Saarinen V., Hovatta T., 2005, A&A, 440, 409

Ulvestad J. S., Johnston K. F., Weiler K. W., 1983, ApJ, 266, 18

Villata M. et al.2007, A&A, 464, 5

Wehrle A. E., Piner B. G., Unwin S. C., Zook A. C., Xu W., Marscher A. P., Terasranta H., Valtaoja E., 2001, ApJS, 133, 297

Zhou J. F., Hong X. Y., Jiang D. R., Venturi T., 2000, ApJ, 541, L13

This paper has been typeset from a TEX/LATEX file prepared by the author.